Journal of Marine Research, 60, 855–886, 2002

Fe redox cycling in Iberian continental margin sediments (NE Atlantic)

by Claar van der Zee[1,2], Wim van Raaphorst[1,3] and Willem Helder[1]

ABSTRACT

In this paper, data are presented on the vertical distribution of pore water Fe^{2+}, ferrozine-extractable Fe^{2+} and solid phase Fe in sediments along four across-slope transects including the Nazaré canyon at the Iberian margin. Sorbed Fe^{2+} cannot be measured directly and is operationally defined as the fraction that can be extracted with ferrozine. Our objectives were (1) to investigate the potential role of Fe^{2+} sorption in the Fe redox cycle, (2) to quantify Fe redox cycling and (3) to determine its rate limiting factors, with emphasis on differences between stations across the slope and in the canyon. In all sediments pore water Fe^{2+} and ferrozine-extractable Fe^{2+} concentrations increased simultaneously with depth until a maximum was reached and upon which the pore water Fe^{2+} concentration rapidly declined, presumably due to precipitation as iron-sulfide. The ferrozine-extractable Fe^{2+} concentration, however, either slowly diminished or remained unchanged when going deeper into the sediment, suggesting ongoing reaction at the sorption surfaces or much slower desorption than adsorption kinetics. Upon Fe reduction, Fe^{2+} is released into the pore water where it either directly precipitates and/or adsorbs onto available surfaces of the sediment matrix, including organic matter. Through sorption, authigenic ferrous mineral formation is delayed and Fe^{2+} may be transported deeper into the sediment. There, sorbed Fe^{2+} can act as a deep source for authigenic ferrous mineral formation. A simple steady-state model was formulated that includes Fe^{2+} sorption as a first-order kinetic reaction to estimate Fe reaction rates. Fe oxidation and reduction rates were most intense at the shelf, where organic carbon mineralization rates are high, and decreased with water depth. In the canyon, where deposition fluxes were high, Fe reaction rates increased with water depth until a maximum at the foot of the canyon at 3097 m and decreased again to the abyssal at 4280 m. Turnover times estimated for pore water Fe^{2+}, ferrozine-extractable Fe^{2+} and solid phase Fe both in the oxidized and reduced layer indicated that sediment mixing was the most important rate limiting factor for Fe cycling at all stations of the Iberian margin. The contribution of Fe reduction to organic matter mineralization was 5% at the 104-m and 113-m stations on the main transect and 6% at the 3097-m station at the foot of the canyon. At the other stations Fe reduction contributed less than 4% to the mineralization of organic matter.

1. Department of Marine Chemistry and Geology, Royal Netherlands Institute for Sea Research, P. O. Box 59, 1790 AB Den Burg, Texel, The Netherlands.

2. Present address: Laboratory of Chemical Oceanography and Water Geochemistry, Université Libre de Bruxelles, Campus de la Plaine CP 208, Boulevard du Triomphe, 1050 Brussels, Belgium. ***e-mail: cvdzee@ulb.ac.be***

3. Deceased.

1. Introduction

Fe reduction may be coupled to the bacterial oxidation of organic matter (Lovley and Phillips, 1988) or to the oxidation of reduced solutes such as sulfides (Rickard, 1995). Fe^{2+} released into the pore water upon solid phase Fe(III) reduction can be complexed by organic ligands (Luther III *et al.,* 1992; 1996), but a large part may sorb onto the ubiquitous surfaces of the sediment matrix. Furthermore, it may precipitate as authigenic ferrous minerals or oxidize upon diffusive transport into the oxidized layer. Sorbed Fe^{2+} and solid phase Fe(II) may also be transported into the oxidized layer through sediment mixing and subsequently re-oxidize and precipitate as Fe(III)oxyhydroxide. Sorption of Fe^{2+} plays an important role in catalyzing the reductive dissolution of Fe(III) oxides (Stumm, 1992, Luther III *et al.,* 1996). Sorption of Mn^{2+} onto Mn(IV) oxides has been demonstrated to act as an intermediate between reductive dissolution and release of Mn^{2+} into the pore water (Van der Zee *et al.,* 2001).

In contrast to sorption of other metals, little is known about sorbed Fe^{2+}. Fe(III) oxyhydroxides are known to be important substrates for trace metal sorption in aquatic systems (Tessier *et al.,* 1996). As the commonly applied determination of adsorbed trace metals on Fe oxyhydroxides involves their reductive dissolution, it is not suitable for the determination of sorbed Fe^{2+} (Tessier *et al.,* 1979; 1996). Zhang *et al.* (1995) applied the technique of diffusion gradients in thin films (DGT) to measure *in situ* fluxes of metals. Depending on the metal involved and application time, the DGT technique can be used to measure pore water concentrations (diffusive flux is dominant) or to calculate fluxes from solid phase to solution. In the case of Fe^{2+}, partial re-supply from the solid phase to the solution was observed in Lake Esthwaite Water (UK), suggesting that reversible sorption processes controlled pore water concentrations (Zhang *et al.,* 1995).

In most diagenetic models, Fe^{2+} sorption is neglected (Aller, 1980; Dhakar and Burdige, 1996) or described as an instantaneous equilibrium process with pore water Fe^{2+} (Slomp *et al.,* 1997). In the multicomponent reactive transport model STEADYSED, Fe^{2+} sorption is included as a surface-controlled equilibrium process and adsorbed Fe^{2+} profiles are simulated assuming Mn oxides, Fe oxyhydroxides, minerals and organic material as the substrate surfaces controlling Fe^{2+} sorption (Van Cappellen and Wang, 1996; Wang and Van Cappellen, 1996). Simulations with this model showed the importance of adsorption-desorption of Fe^{2+} in the Fe redox cycling and the impact on pore water alkalinity and pH (Wang and Van Cappellen, 1996). Van Cappellen and Wang (1996) simulated a profile of adsorbed Fe^{2+} and emphasize the importance of heterogeneous oxidation, i.e. oxidation with surface-bound Fe^{2+} as reactant instead of pore water Fe^{2+}. Field data including profiles of adsorbed Fe^{2+} to confirm the modeling results are, however, lacking, so far.

We measured the vertical distribution of dissolved Fe^{2+}, loosely sorbed Fe^{2+} (through extraction with ferrozine), and solid phase Fe in sediments from the Iberian continental margin including the Nazaré canyon. A simple steady state model was formulated to estimate the depth-integrated rates of Fe(III) reduction and Fe(II) oxidation. Our first objective was to study the role of Fe^{2+} sorption in the redox cycling of Fe in natural

continental margin sediments. Furthermore, we wanted to quantify Fe redox cycling and determine its rate limiting factors, contrasting stations at the shelf and slope of the Iberian continental margin to the Nazaré canyon. First, we will discuss the role of loosely sorbed Fe^{2+} in the Fe cycle, possible substrates for Fe^{2+} sorption and the rate-limiting factor for Fe cycling estimated from the model results. Then, we will compare the canyon with the rest of the Iberian margin and the Iberian margin with the rest of the global oceans.

2. Research area

Our research area comprised the Iberian continental margin in the northeastern Atlantic (Fig. 1). Stations were located at different depositional areas, on four transects across the margin including one in the Nazaré canyon, and were sampled during 2 cruises within the Ocean Margin Exchange Project (OMEX-II) in August 1998 and May 1999. Characteristics of the visited stations are listed in Table 1. Organic carbon contents range from 0.33 to 4.58 wt% C. The northern most La Coruña transect is characterized by a gradual decreasing water depth, whereas the slope is steeper at both the Vigo transect, north of Vigo, and the main transect situated south of Vigo. As canyons are important conduits for particle transport from the shelf directly to the deep-sea (Durieu de Madron *et al.,* 1999; Monaco *et al.,* 1999; Sanchez-Cabeza *et al.,* 1999), we selected an additional transect in the Nazaré canyon further to the south (Schmidt *et al.,* 2001), where four stations were sampled inside the canyon and an additional two on the adjacent shelf. Details on carbon cycling at the Iberian margin are discussed in Epping *et al.* (2002). Benthic oxygen fluxes on the shelf range from 2 to 3.6 mmol $O_2\ m^{-2}\ d^{-1}$ exponentially decreasing to 0.6 mmol $O_2\ m^{-2}\ d^{-1}$ at 3000-m water depth at the non-canyon transects. In the canyon the benthic oxygen fluxes decrease from 4.9 at 344-m water depth to 2.3 at 3097 m and 0.9 mmol $O_2\ m^{-2}\ d^{-1}$ at 4280 m.

3. Materials and methods

a. Sediment handling

Sediment cores were taken with a multi-corer and processed directly at *in situ* temperature. Four sediment cores were sliced simultaneously for pore water collection with a hydraulic core-slicer developed at NIOZ (Van der Zee *et al.,* 2001) to obtain accurate high spatial resolution at particularly the sediment-water interface. The sediment was sectioned in 2.5-mm slices in the upper 10 mm of the sediment, in 5-mm slices from 10 to 30 mm, in 10-mm slices from 30 to 60 mm and in 20-mm slices further down. The sediment slices were pooled and centrifuged (3000 rpm, 10 min) for pore water extrusion. Pore water was filtered (0.45 μm) and analyzed for nitrate and iron shipboard on a TRAACS-800 auto-analyzer. Nitrate was analyzed according to the method of Strickland and Parsons (1972). Aliquots for iron were acidified to pH 2 and analyzed according to the method of Stookey (1970). After pore water collection the sliced sediment was stored frozen (−20°C) until further analysis for solid phase iron at the NIOZ laboratory.

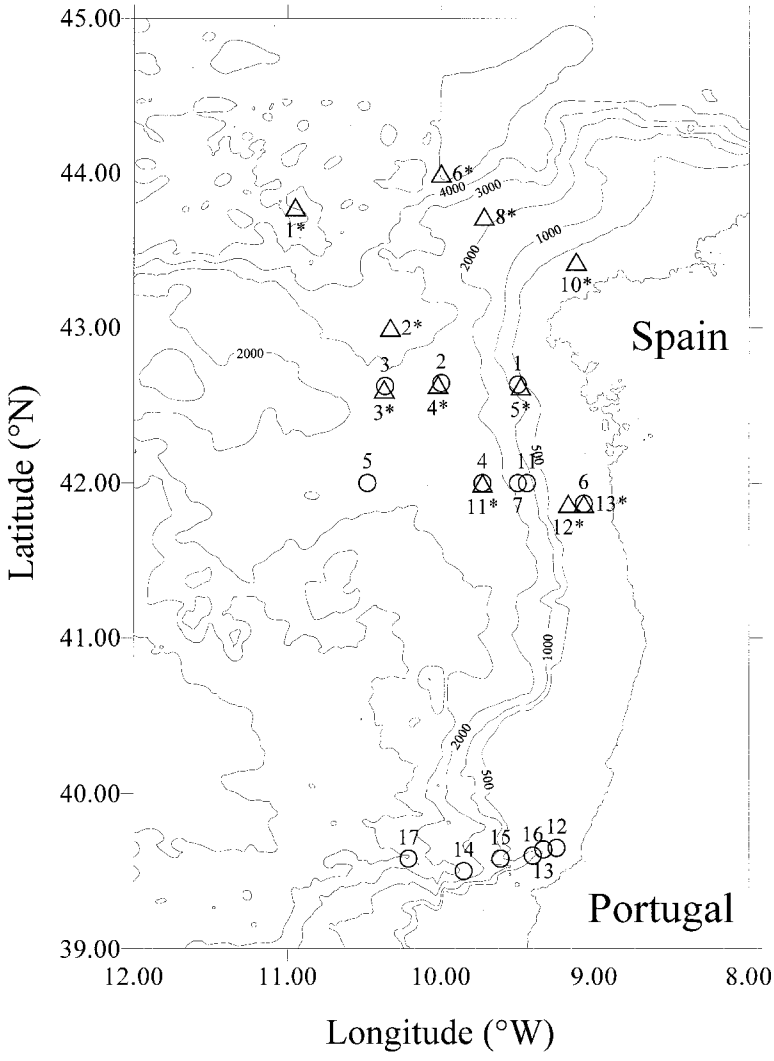

Figure 1. Map of the Iberian Margin indicating positions of sampled stations in 1998 (triangles, numbers with asterisk) and 1999 (circles, numbers without asterisk).

Freeze-dried and ground sediment was extracted with 1N HCl (24 hrs, 20°C) for reactive solid phase Fe (Canfield, 1988; Slomp *et al.,* 1997). Fe was measured in 1N HCl (solid phase Fe) and ferrozine (sorbed Fe^{2+}, see below) extracts by flame AAS. Porosity was determined from the weight loss of the sediment after drying at 60°C assuming a sediment dry density of 2.65 g cm^{-3}. Sediment cores were not sectioned entirely anoxic and therefore small oxidation artifacts may have affected the pore water profiles of iron (at most 10% of the dissolved Fe).

Table 1. Name, water depth, geographical position, bottom water (BW) temperature and oxygen concentration and organic carbon content of the visited stations, number 121-stations are visited in August 1998 and number 138-stations are visited in May 1999.

Station	Water depth (m)	Lat. °N	Long. °W	BW Temp (°C)	BW O_2 (μM)	Corg* (wt %)
I La Coruña Transect						
121-10	175	43.26	09.07	12.1	225	0.33
121-08	2109	43.43	09.43	3.2	250	1.04
121-06	4908	44.00	10.00	3.1	245	0.72
121-01	4941	43.47	10.57	3.1	245	0.45
II Vigo Transect						
138-01	213	42.38	09.28	12.1	213	0.47
121-05	223	42.38	09.29	12.0	223	0.62
138-02	2164	42.38	10.00	3.4	249	1.35
121-04	2213	42.38	10.01	3.2	250	1.16
138-03	2932	42.37	10.22	2.5	243	1.01
121-03	2926	42.36	10.22	3.1	243	0.87
121.02	3371	43.00	10.20	3.1	245	1.08
III Main Transect						
121-13	104	41.52	09.04	12	235	4.58
138-06	113	41.52	09.04	12.5	210	4.46
121-12	123	41.52	09.10	12.1	230	0.42
138-11	932	42.00	09.26	—	—	1.41
138-07	1387	42.00	09.28	10.3	188	1.99
138-04	2060	42.00	09.44	3.8	247	1.17
121-11	2073	42.00	09.44	3.4	255	1.41
138-05	2853	42.00	10.30	2.6	241	0.88
IV Nazaré Canyon Transect						
138-13	137	39.39	09.20	12.8	209	0.86
138-12	344	39.39	09.15	12.2	206	3.46
138-15	396	39.35	09.37	11.6	200	1.04
138-16	890	39.36	09.24	11.0	189	3.12
138-14	3097	39.31	09.51	2.4	243	3.67
138-17	4280	39.35	10.17	2.1	243	2.56

*Organic carbon content in 0–2.5 mm interval

b. Sorbed Fe^{2+}

The Fe(II)-complexing agent ferrozine that is often used in Fe(III) reduction assays to extract Fe^{2+} from the sediment matrix (Sørensen, 1982; Stookey, 1970) was applied to determine sorbed Fe^{2+}. Thawed wet sediment from the 1998 cruise was extracted with 1 g/L ferrozine in 50 mM HEPES (pH 7.0) for 5 min in the laboratory. On the 1999 cruise an additional core was sliced and fresh wet sediment was extracted with 1 g/L ferrozine in 50 mM HEPES (pH 7) for 5 min. directly on board. The extract was filtered (0.45 μm), acidified and stored at 4°C. Corrections were made for the pore water Fe^{2+} in the extract, using pore water data and porosity values. Tügel *et al.* (1986) extended this technique with

the addition of 1N HCl for 15 s before adding the buffered ferrozine solution to release Fe^{2+} associated with acid-soluble material like FeS. Lovley and Phillips (1986) applied the procedure as developed by Sørensen (1982) with and without first extracting the samples with 0.5N HCl and concluded that the hydrochloric acid extraction method was superior to ferrozine extraction in extracting solid Fe^{2+} forms, including FeS, produced upon Fe(III) reduction. We applied the technique without the HCl addition to extract sorbed Fe^{2+} while minimizing the dissolution of other authigenic Fe^{2+} phases (e.g. iron monosulfide, iron carbonate, magnetite, green rusts and iron bound in clay minerals) produced upon Fe reduction.

Triplicate samples of iron monosulfide (FeS, Aldrich 34,316-1, 99.9%), magnetite (Fe_3O_4, Alfa Aeser 012374, 97%) and siderite (natural $FeCO_3$, collection of S.J. van der Gaast, NIOZ) were extracted with the buffered ferrozine solution (1 g/L ferrozine in 50 mM HEPES pH 7.0). After 5 min. less than 1% Fe was leached from the iron monosulfide, magnetite and siderite, probably from outer reactive mineral surfaces. The extraction procedure was not tested on green rusts or reduced iron bound in clay minerals. It is highly unlikely, however, that buffered ferrozine (pH 7.0) could extract substantial amounts of structural Fe^{2+} from the clay mineral lattice within 5 min. Three kinds of mineral dissolution can be distinguished, i.e. proton-, ligand- and reductant-promoted dissolution (Sulzberger *et al.,* 1989). Both ferrozine and oxalate operate as ligands. Oxalate liberates less than 3% of the total iron from clay minerals, whereas solutions of 1N HCl and dithionite-acetate-citrate (pH 4.8) can leach up to 32% of the total Fe from chlorite, nontronite and biotite (Canfield, 1988; Kostka and Luther, 1994). Natural green rusts in marine sediments have not been positively identified yet (Hansen *et al.,* 1994). Green rust has been detected, however, as corrosion product of cast iron pipes (Stampfl, 1969), in an ochre sludge (Koch and Mørup, 1991) and in a reductomorphic soil (Trolard *et al.,* 1997). The buffered ferrozine solution may extract some iron from green rusts if present.

Batch adsorption experiments were conducted with anoxic sediment (80–100 mm slice) from the 344-m station at the Nazaré Canyon Transect in N_2-purged seawater buffered with 50 mM HEPES pH 7.8. Canfield *et al.* (1993) reported difficulties to control the pH satisfactory in their Fe adsorption experiments, therefore the seawater was buffered with HEPES (*cf.* Burdige and Kepkay, 1983). Single additions of Fe^{2+} were made using a particle concentration in the experiments of $\sim$15 g L^{-1}. Solutions were left to equilibrate for 30 minutes, which was found to be the maximum time for the best recovery in separate experiments. Dissolved Fe^{2+} was measured in the supernatant and Fe^{2+} sorbed onto the sediment was determined with the ferrozine extraction procedure. Control experiments both without sediment and without Fe^{2+} addition were performed. The observed isotherm (Fig. 2) could be described with the Freundlich equation with the amount of sorbed $Fe^{2+} = K_F \times [Fe^{2+}]^{1/n}$. The Freundlich constant, K_F, is 0.60 $dm^3\ g^{-1}$ and the Freundlich exponent, n, is 2.72. The concentrations used in the adsorption experiment span the same range as found in the sediment. Mass balance calculations indicated that the buffered ferrozine reagents recovered only 35% of the added Fe^{2+}, using longer equilibration times

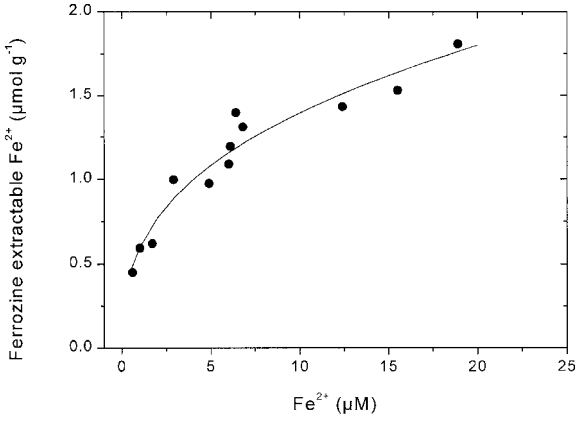

Figure 2. Isotherm data from the adsorption experiment (dots) fit with the Feundlich equation (line).

than 30 min resulted in a lower recovery while control experiments without sediment did not loose their Fe^{2+}. This indicates that the added Fe^{2+} may react with substances (e.g. free sulfides) in the thawed sediment in short time, resulting in strong bonds that could not be disrupted with ferrozine. Alternatively, the Fe^{2+} may become more strongly bound upon initial sorption to the reactive surfaces, suggesting a transition from loosely sorbed Fe^{2+} (extractable with ferrozine) to tightly sorbed Fe^{2+} in short time. Such reactions affect the measurement of sorbed Fe^{2+} most strongly in the non-steady state situation after the Fe^{2+} addition, and was probably less pronounced in the shipboard assay of the natural sediment. Without further knowledge we conclude that the ferrozine extraction operationally defines the pool of sorbed Fe^{2+}, similar to most other chemical extraction techniques for solid metal compounds. We will refer to the buffered ferrozine-extractable Fe^{2+} as loosely sorbed Fe^{2+}.

4. Model

Early diagenetic models have been developed that couple the diagenesis of Fe to the cycles of C, N, O, S and Mn (e.g. Dhakar and Burdige, 1996; Van Cappellen and Wang, 1996). We developed a simple one-dimensional steady state diffusion model that includes ferrozine-extractable Fe^{2+} as a proxy for loosely sorbed Fe^{2+}, similar to the model used to describe Mn redox cycling in the same sediments (Van der Zee *et al.*, 2001). The model describes Fe^{2+} sorption as a net first-order kinetic process, avoiding complications associated with separate back and forward reaction terms as well as with saturating sorption surfaces. We are aware that this is a strong simplification, but it allowed us to reduce the number of variables compared to coupled models, to limit the uncertainties in data of other elements that could affect the modeling of Fe, and to better focus on sorption and the Fe redox cycle while staying as close as possible to the experimental data set.

A list of model parameters is given in Table 2. The molecular sediment diffusion

Table 2. Name, unit and function of model parameters.

Name	Unit	Function
D_s	$m^2\ d^{-1}$	Molecular sediment diffusion coefficient
D_b	$m^2\ d^{-1}$	Bioturbation coefficient
ω	$m\ d^{-1}$	Sedimentation rate
x	m	Depth in sediment
L	m	Depth of Fe redox boundary
ϕ	—	Sediment porosity
ρ	$g\ cm^{-3}$	Average density of the sediment
ϑ	$g\ cm^{-3}$	Conversion factor between pore water and solid or loosely sorbed phase
C_I	$mol\ m^{-3}$	Pore water Fe^{2+} concentration in the oxidized layer
C_{II}	$mol\ m^{-3}$	Pore water Fe^{2+} concentration in the reduced layer
A_I	$\mu mol\ g^{-1}$	Loosely sorbed Fe^{2+} concentration in the oxidized layer
A_{II}	$\mu mol\ g^{-1}$	Loosely sorbed Fe^{2+} concentration in the reduced layer
S_I	$\mu mol\ g^{-1}$	Solid phase Fe concentration in the oxidized layer
S_{II}	$\mu mol\ g^{-1}$	Solid phase Fe concentration in the reduced layer
C_a	$mol\ m^{-3}$	Pore water equilibrium concentration for precipitation
A_{eq}	$\mu mol\ g^{-1}$	Loosely sorbed Fe^{2+} concentration at which no further reactions occur
S_{eq}	$\mu mol\ g^{-1}$	Solid phase Fe concentration at which no further reactions occur
k_{oxc}	d^{-1}	Dissolved Fe^{2+} oxidation rate constant
k_{oxa}	d^{-1}	Sorbed Fe^{2+} oxidation rate constant
k_r	d^{-1}	Reduction rate constant
k_s	d^{-1}	Sorption rate constant
k_a	d^{-1}	Dissolved Fe^{2+} precipitation rate constant
k_p	d^{-1}	Sorbed Fe^{2+} precipitation rate constant
$J_{Ax=0}$	$\mu mol\ m^{-2}\ d^{-1}$	Flux of loosely sorbed Fe^{2+} at the sediment-water interface
$J_{Sx=0}$	$\mu mol\ m^{-2}\ d^{-1}$	Flux of solid phase Fe at the sediment-water interface

coefficient (D_s in $m^2\ d^{-1}$), mixing coefficient (D_b in $m^2\ d^{-1}$), all reaction rate constants (k in d^{-1}), sediment porosity (ϕ in $m^3\ m^{-3}$) and the sedimentation rate (ω in $m\ d^{-1}$) are assumed to be depth-independent. Irrigation is not included, as no data are available on this process. The sediment was divided into an oxidized and a reduced layer. The depth of the redox boundary (L) is given by the depth where the nitrate concentration is <5 μM (maximum nitrate concentration allowing Fe(III) reduction between 1–10 μM; Van Cappellen and Wang, 1995). In the oxidized layer, oxidation of both dissolved and ferrozine-extractable Fe^{2+} takes place, described as first-order processes with k_{oxc} and k_{oxa} as the oxidation rate constants, respectively. Pore water Fe^{2+} concentrations (C_I and C_{II}) have units in $mol\ m^{-3}$, ferrozine-extractable Fe^{2+} (A_I and A_{II}) and solid phase Fe (S_I and S_{II}) concentrations are in $\mu mol\ g^{-1}$. For the conversion between pore water and solid phase Fe or ferrozine-extractable Fe^{2+} the factor ϑ (gram of dry sediment per cm^3 of pore water) is used: $\vartheta = \rho[(1 - \phi)/\phi]$, where ρ is the average dry density of the sediment (2.65 $g\ cm^{-3}$). Differential equations for dissolved Fe^{2+} (C_I), ferrozine-extractable Fe^{2+}

(A_I), and solid phase Fe (S_I) in the oxidized layer as a function of depth in the sediment (x) are:

$$[D_b + D_s]\frac{\partial^2 C_I}{\partial x^2} - \omega\frac{\partial C_I}{\partial x} - k_{oxc}C_I = 0 \quad (1)$$

$$D_b\frac{\partial^2 A_I}{\partial x^2} - \omega\frac{\partial A_I}{\partial x} - k_{oxa}A_I = 0 \quad (2)$$

$$D_b\frac{\partial^2 S_I}{\partial x^2} - \omega\frac{\partial S_I}{\partial x} + k_{oxa}A_I + \frac{k_{oxc}}{\vartheta}C_I = 0 \quad (3)$$

Note that desorption of ferrozine-extractable Fe^{2+} as a possible intermediate step before oxidation to Fe(III) oxides is not taken into account.

In the reduced layer, Fe(III) reduction, Fe^{2+} sorption and precipitation occur. Production of dissolved Fe^{2+} due to solid phase Fe(III) reduction is described as a first-order process with k_r as the reduction rate constant. Removal of dissolved and ferrozine-extractable Fe^{2+} due to authigenic mineral formation is described as a first-order process with k_a and k_p as the precipitation rate constants, respectively. The "precipitation" of loosely sorbed Fe^{2+} is assumed to occur at the sorption surfaces, but Fe^{2+} desorption may be involved prior to rapid precipitation in authigenic ferrous minerals at nearby sites. The pore water and ferrozine-extractable Fe^{2+} equilibrium concentrations for precipitation are C_a and A_{eq}, respectively. Sorption of dissolved Fe^{2+} is described as a first-order process with k_s as the sorption rate constant. The solid phase Fe concentration at which no further reaction occurs is S_{eq}. Differential equations for dissolved Fe^{2+} (C_{II}), ferrozine-extractable Fe^{2+} (A_{II}) and solid phase Fe (S_{II}) in the reduced layer are:

$$[D_b + D_s]\frac{\partial^2 C_{II}}{\partial x^2} - \omega\frac{\partial C_{II}}{\partial x} - k_s C_{II} + k_r\vartheta(S_{II} - S_{eq}) - k_a(C_{II} - C_a) = 0 \quad (4)$$

$$D_b\frac{\partial^2 A_{II}}{\partial x^2} - \omega\frac{\partial A_{II}}{\partial x} + k_s\frac{C_{II}}{\vartheta} - k_p(A_{II} - A_{eq}) = 0 \quad (5)$$

$$D_b\frac{\partial^2 S_{II}}{\partial x^2} - \omega\frac{\partial S_{II}}{\partial x} - k_r(S_{II} - S_{eq}) = 0 \quad (6)$$

The 6 differential equations were analytically solved assuming continuity of concentrations ($C_I = C_{II}$, $A_I = A_{II}$ and $S_I = S_{II}$) and fluxes at the redox boundary and specific conditions at the external boundaries, i.e. the sediment-water interface and at infinite depth (see Appendix). At the sediment-water interface the concentration of dissolved Fe^{2+} equals that in the overlying water (C_0 is set at 0 μM), the flux of solid phase Fe(III) is $J_{Sx=0}$ (μmol m^{-2} d^{-1}) and the flux of ferrozine-extractable Fe^{2+} ($J_{Ax=0}$) is zero. At infinite depth the concentrations of C_{II}, A_{II} and S_{II} converge to C_a, A_{eq} and S_{eq}, respectively, as their fluxes diminish. Variance-weighted sums of squares (Slomp *et al.*,

1997) for dissolved and ferrozine-extractable Fe^{2+} and solid phase Fe(III) were minimised simultaneously, while five parameters (k_r, k_s, k_a, k_p and $J_{Sx=0}$) were varied to fit the model to the data using the Excel™ solver routine. The mechanistic coupling of the three profiles in the models gives a strong constraint on the five adjustable parameters.

The values of fixed parameters are given in Table 3. As no literature data on the oxidation rate of ferrozine-extractable Fe^{2+} in marine sediments were available, we assumed the rate constant for ferrozine-extractable Fe^{2+} oxidation to be equal to the rate constant for dissolved Fe^{2+} oxidation. For the 2109-m station on the La Coruña transect and the 123-m station on the main transect for which ferrozine-extractable Fe^{2+} data were not available, the more simple Fe model of Slomp *et al.* (1997), which does not contain ferrozine-extractable Fe^{2+}, was applied to the profiles of solid phase Fe(III) and pore water Fe^{2+} to assess Fe(III) reduction and Fe(II) oxidation rates.

5. Experimental results

At low concentrations of nitrate (<5 μM), Fe^{2+} may start to accumulate in the pore water. Therefore, nitrate profiles are suitable to describe the relevant Fe redox conditions in the sediment. The maximum nitrate concentration as well as the depth in the sediment where nitrate is depleted increased with water depth. At the *La Coruña transect,* the shallow 175-m station was rapidly depleted in nitrate (Fig. 3). At the two deepest stations, the nitrate concentration was higher than 10 μM throughout the sampled interval and therefore Fe(III) reduction is not expected to occur. Nitrate was depleted around 5 cm depth in the sediment at the two shallow stations on the *Vigo transect,* indicating that Fe reduction may occur. The two stations around 2200 m showed the depletion of nitrate at the bottom of the sampled interval, therefore Fe(III) reduction is expected to have started just below that interval. The nitrate concentration at the three deepest stations was too high throughout the sampled interval for Fe(III) reduction to occur. At the *main transect,* the shallow stations were rapidly depleted in nitrate. At the two stations around 2000-m water depth, low nitrate concentrations at the bottom of the sampled intervals suggest it to be close to the Fe redox boundary. At the *canyon transect,* the same trend was observed, i.e. the nitrate concentration and the depth where nitrate was depleted both increased with water depth, however, nitrate was more rapidly depleted in the canyon stations compared to stations at the same water depth on the margin.

Fe profiles of the stations on the *La Coruña transect* are given in Figure 4. At the shallow station pore water and ferrozine-extractable Fe^{2+} increased simultaneously until the pore water maximum was reached at 120 mm depth, after which the ferrozine-extractable Fe^{2+} concentration remained constant but the pore water Fe^{2+} concentration decreased. The deeper part of the profile suggest precipitation of dissolved Fe^{2+} that is not accompanied by desorption of Fe^{2+}. The pore water Fe^{2+} concentrations as well as the solid Fe content decreased going down slope. At the two shallowest stations on the *Vigo transect* (Fig. 5), both ferrozine-extractable and dissolved Fe^{2+} concentrations decreased below 5–8 cm depth, but pore water Fe^{2+} diminished most rapidly. The relevant redox boundary was too

Table 3. Fixed parameters used in model calculations.

Water depth (m)	(1) k_{oxc} (d^{-1})	(2) k_{oxa} (d^{-1})	(3) D_b ($m^2\ d^{-1}$)	(4) D_s ($m^2\ d^{-1}$)	(5) ω ($m\ d^{-1}$)	(6) L (m)	(7) C_a (μM)	(8) A_{eq} (μmol g^{-1})	(9) S_{eq} (μmol g^{-1})
I La Coruña Transect									
175	10	10	1.95E-7	1.61E-5	9.86E-8	0.04	1	0.39	240
2109	10	—	3.04E-8	2.50E-5	1.48E-7	0.075	5	—	90
II Vigo Transect									
223	10	10	2.30E-7	1.70E-5	1.37E-7	0.01	0.1	0.1	122
III Main Transect									
104	10	10	5.48E-7	2.11E-5	1.37E-7	0.0015	6	0.3	150
113	10	10	5.48E-7	2.35E-5	1.37E-7	0.015	2	0.9	195
123	10	—	5.48E-7	2.35E-5	1.37E-7	0.01	2	—	140
932	10	10	3.32E-8	1.97E-5	2.74E-7	0.03	17	0.25	107
1387	10	10	1.07E-8	2.10E-5	2.74E-7	0.03	10	0.8	130
2060	10	10	2.19E-9	2.02E-5	2.55E-7	0.095	2	0.2	59
2073	10	10	2.47E-9	2.02E-5	2.55E-7	0.095	1.5	0.2	130
IV Nazaré Canyon Transect									
137	10	10	1.37E-7	2.11E-5	1.37E-7	0.025	4	0.2	316
396	10	10	1.84E-7	2.01E-5	2.74E-7	0.03	1	0.8	121
344	10	10	1.04E-7	2.80E-5	2.74E-6	0.01	1.5	3.3	242
890	10	10	1.10E-7	2.77E-5	2.74E-7	0.0275	22	4.17	208
3097	10	10	2.74E-7	1.91E-5	2.74E-6	0.0225	100	3.4	207
4280	10	10	6.58E-8	1.20E-5	2.74E-7	0.055	20	0.2	120

(1) k_{oxc} is set at 10 d^{-1} (Slomp *et al.*, 1997) (2) k_{oxa} is set to 10 d^{-1} (see text) (3) D_b is the mixing coefficient taken from Van der Zee *et al.*, 2001), except the D_b of the 104-m station, which is set equal to the D_b of the 113-m station. (4) D_s at 35 PSU, appropriate temperature and corrected for tortuosity (Boudreau, 1997) (5) ω is the sedimentation rate taken from Van der Zee *et al.*, 2001, except the 1387-m station on the main transect (0.01 instead of 0.05 cm yr^{-1}). (6) Nitrate < 5 μM depth (7) Ca is set equal or slightly lower than the deepest Fe^{2+} concentration observed. (8) A_{eq} is set equal or slightly lower than the deepest ferrozine-extractable Fe^{2+} concentration observed. (9) S_{eq} is set equal to the deepest solid Fe concentration measured.

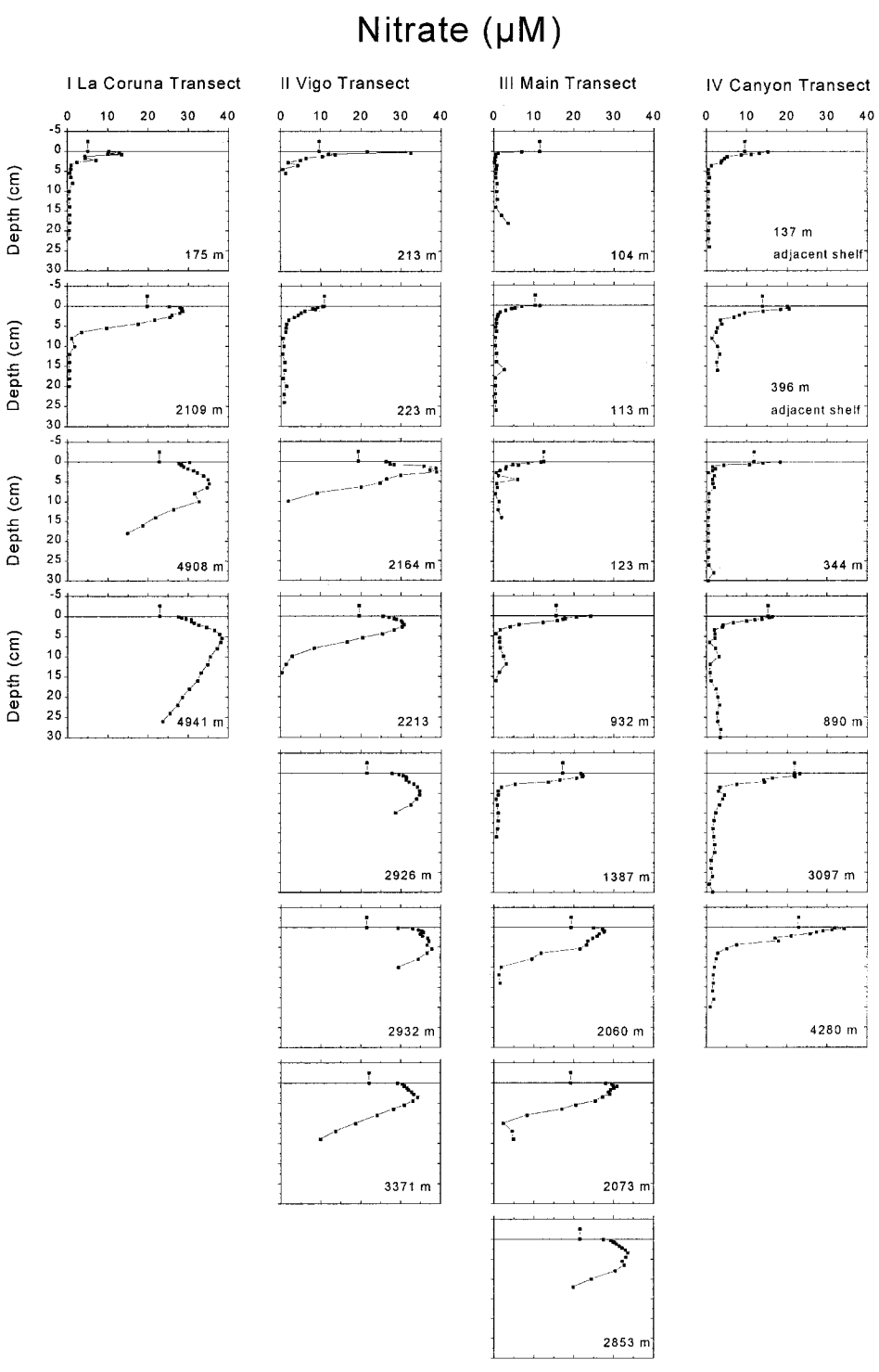

Figure 3. Vertical profiles of pore water nitrate concentrations.

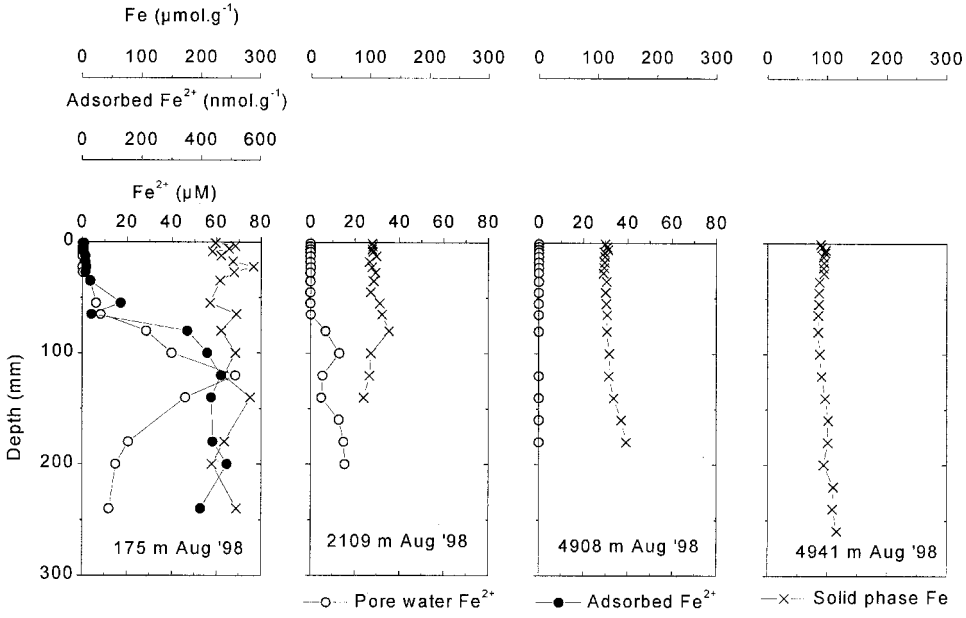

Figure 4. Vertical profiles of pore water Fe^{2+}, ferrozine-extractable Fe^{2+} and solid phase Fe of the stations at the La Coruña transect.

deep at the other stations of this transect to show this phenomenon. The maximum concentrations of ferrozine-extractable and dissolved Fe^{2+} decreased with increasing water depth. Pore water as well as ferrozine-extractable Fe^{2+} concentrations generally decreased from shallow to deeper stations on the *main transect* with a relatively high ferrozine-extractable Fe^{2+} concentration at the 1387-m station (Fig. 6). At all stations pore water and ferrozine-extractable Fe^{2+} increased simultaneously until their maxima were reached, after which both decreased again or remained constant. The concentrations of ferrozine-extractable Fe^{2+} were much higher at the stations at 104, 113 and 1387 m on this transect than at stations on the previously discussed transects. At 2060 and 2073 m, the profiles showed a clear solid phase Fe peak at 100 mm and 80 mm, respectively. Four stations were located in the canyon on the *Nazaré canyons transect,* whereas both the 137- and the 396-m station were situated on the adjacent shelf (Fig. 7). Again, simultaneous increase of pore water and ferrozine-extractable Fe^{2+} was observed, after which pore water Fe^{2+} was removed due to precipitation, but the ferrozine-extractable Fe^{2+} concentration remained constant. Pore water Fe^{2+} concentrations at the stations in the canyon were comparable to stations at shallow water depth on the other transects, except at the canyon station at 3097 m where it was an order of magnitude higher. Ferrozine-extractable Fe^{2+} concentrations were high at the 346-, 890- and 3097-m stations. The solid phase Fe profiles were strongly enriched at the sediment-water interface at the stations in the canyon.

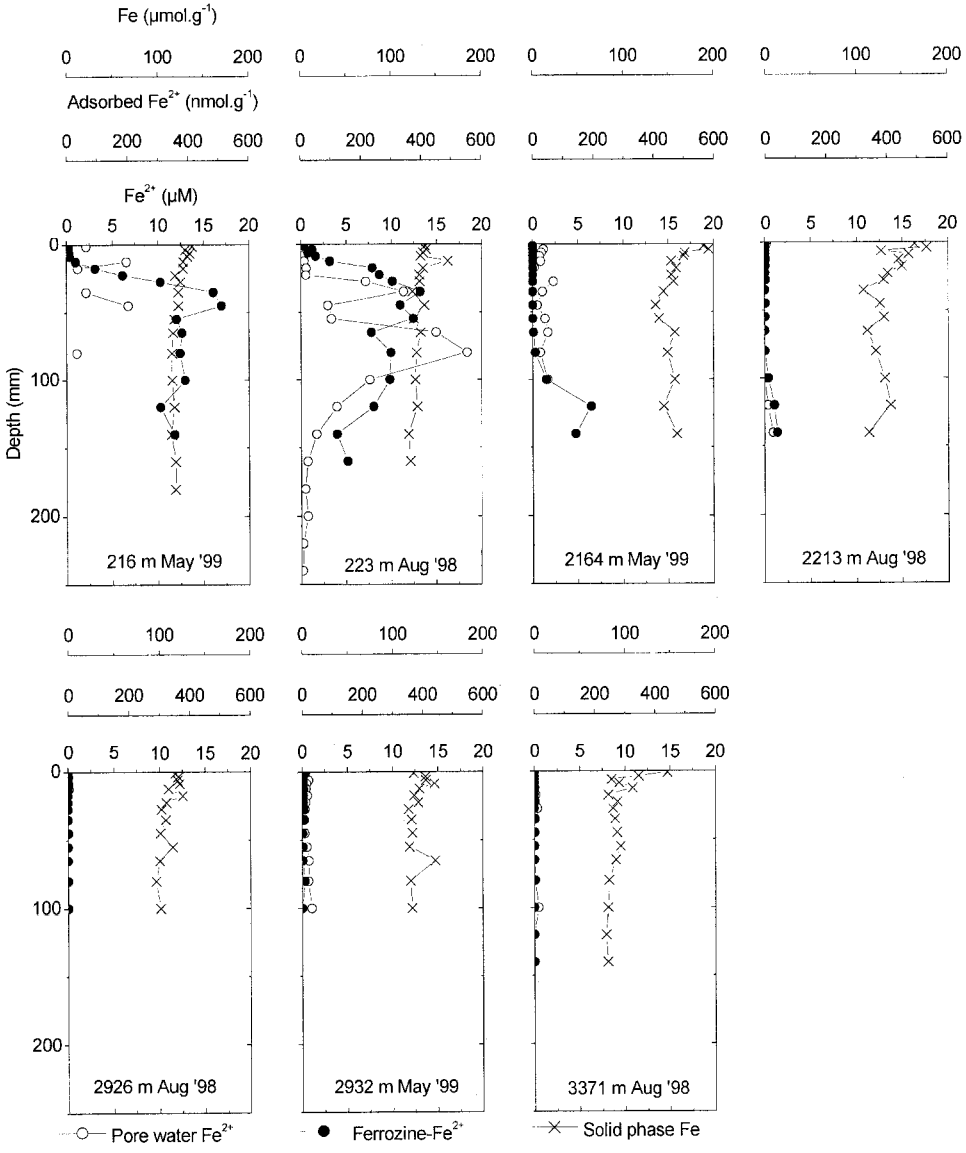

Figure 5. Vertical profiles of pore water Fe^{2+}, ferrozine-extractable Fe^{2+} and solid phase Fe of the stations at the Vigo transect.

6. Model results

The model was applied to stations where dissolved Fe^{2+} accumulated in the pore water. Model fits to the data are given for the *La Coruña* and *Vigo transect* (Fig. 8a), the *main transect* (Fig. 8b) and the *Nazaré canyon transect* (Fig. 8c). The model appears to fit the

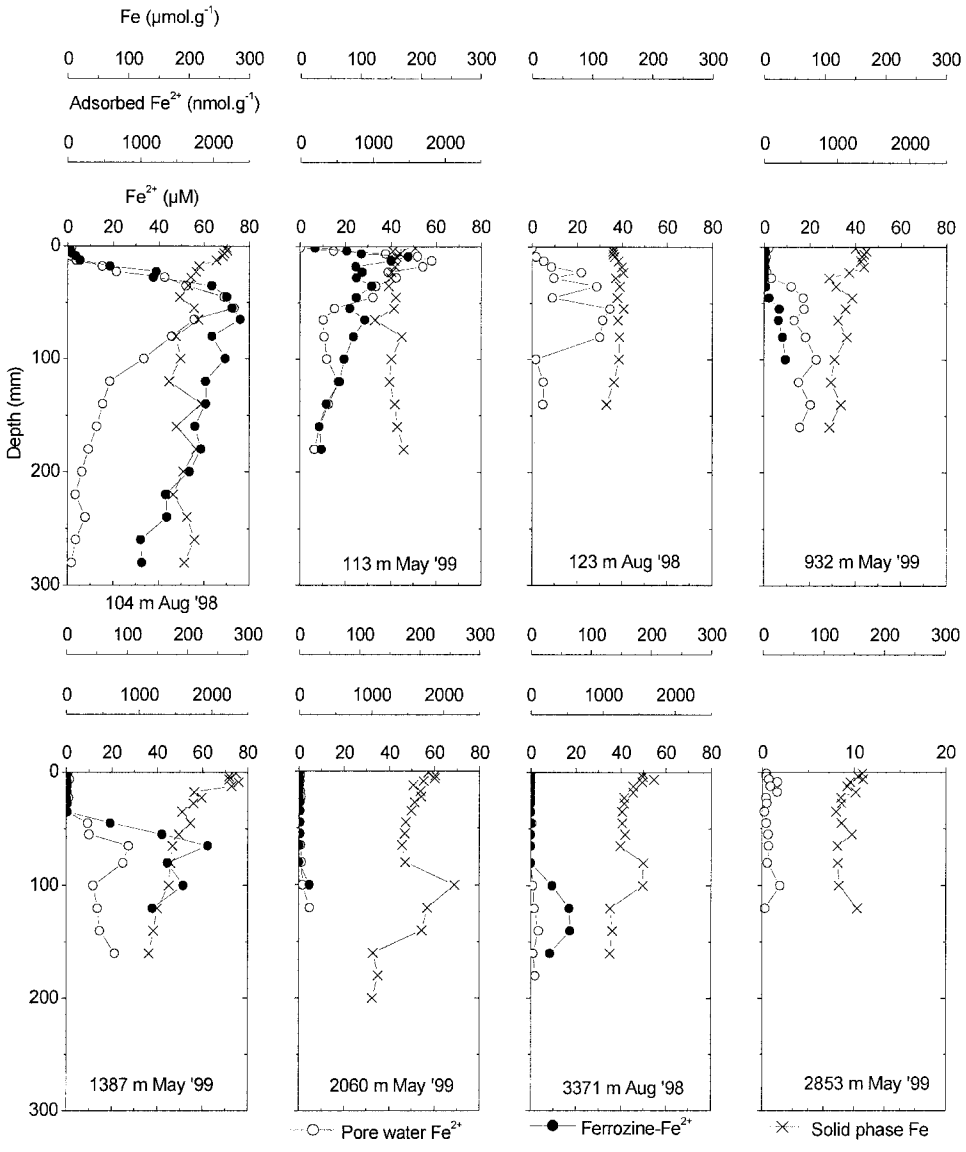

Figure 6. Vertical profiles of pore water Fe^{2+}, ferrozine-extractable Fe^{2+} and solid phase Fe of the stations at the Main transect.

data reasonably well, but there are some shortcomings. It can describe only one Fe^{2+} pore water maximum per profile, however, at several stations double peaks occur. Moreover, the pore water Fe^{2+} maxima are underestimated by the model. Both problems are illustrated by the model fit of the profiles of the 223-m station on the Vigo transect (Fig. 8a). The underestimated pore water maximum is probably due to a more abrupt decline in pore

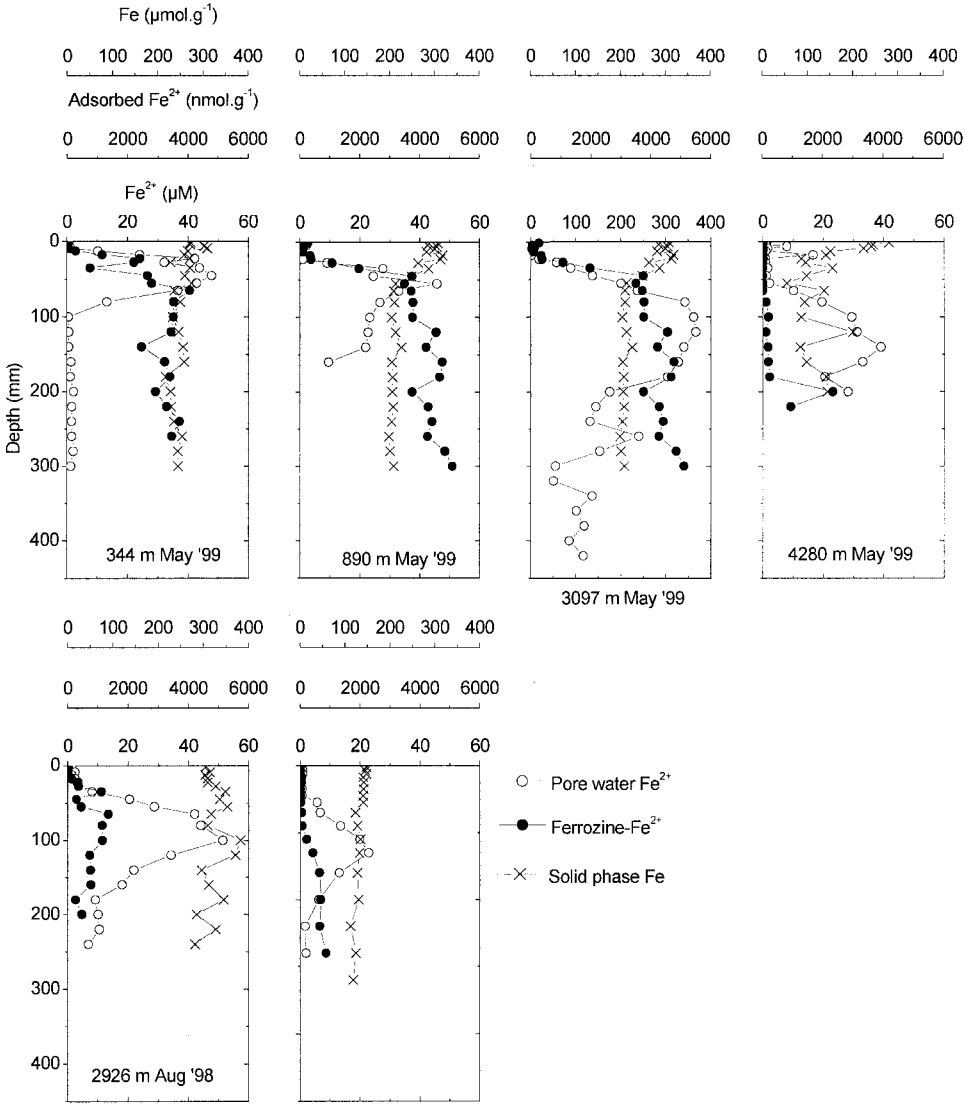

Figure 7. Vertical profiles of pore water Fe^{2+}, ferrozine-extractable Fe^{2+} and solid phase Fe of the stations at the Nazaré canyon transect.

water Fe^{2+} than the model can simulate leading to a model fit in-between the high values of the maximum and the low values deeper in the sediment, e.g. the 344-m station at the Nazaré canyon transect (Fig. 8c). One reason for this discrepancy is that the 1N HCl solution extracts some of the ferrous solid phase Fe (Wallmann *et al.*, 1993) which is attributed here to Fe(III) oxides, thus underestimating the Fe(III) oxide gradient and therefore the Fe reduction rate. However, the main sink of reduced iron in marine

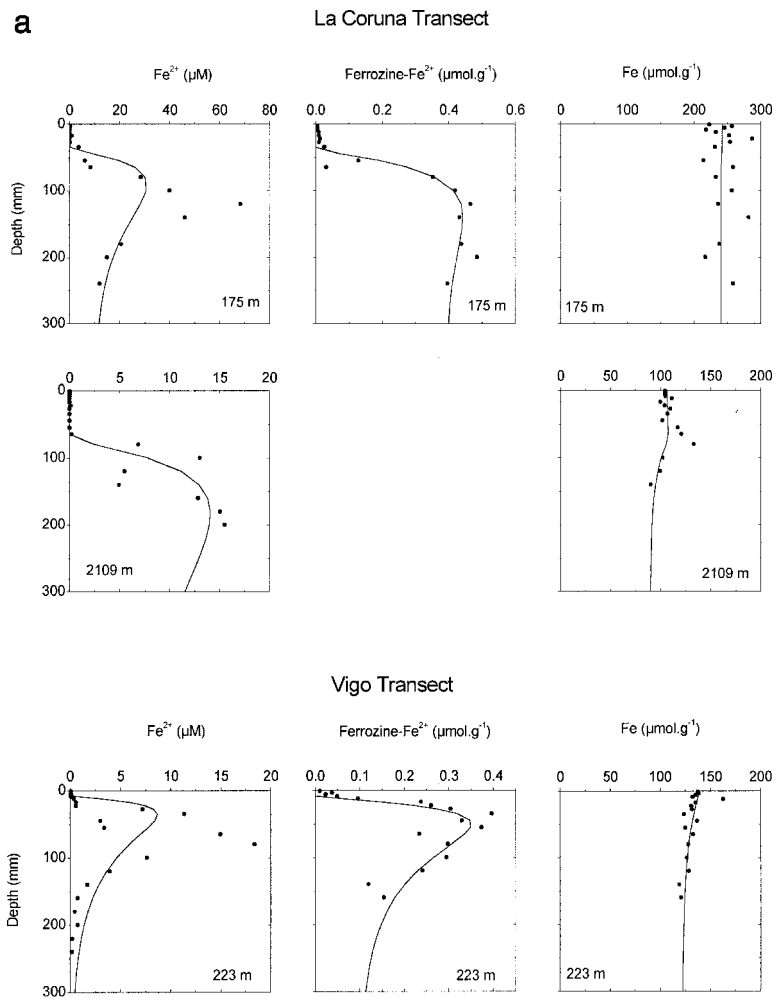

Figure 8. Model fits (lines) to profiles of pore water Fe^{2+}, ferrozine-extractable Fe^{2+} and solid phase Fe (filled circles) of the stations at (a) the La Coruña and Vigo transect, (b) the main transect, and (c) the Nazaré canyon transect.

sediments, pyrite, is not extracted with 1N HCl. The model fit of the deepest station in the canyon is not very good, especially for the solid phase, because the sediment consists of alternating layers of clay and sand containing different amounts of Fe.

The values of the fitted first order rate constants vary several orders of magnitude due to the lumping of a number of factors into one parameter, e.g. Fe(III) oxyhydroxide reactivity, type of reductant, organic matter reactivity, microbial activity and temperature (Table 4; Burdige and Gieskes, 1983; Slomp *et al.*, 1997; Dollhopf *et al.*, 2000). The ranges of all first order rate constants as well as the estimated Fe(III) deposition fluxes ($J_{Sx=0}$) are

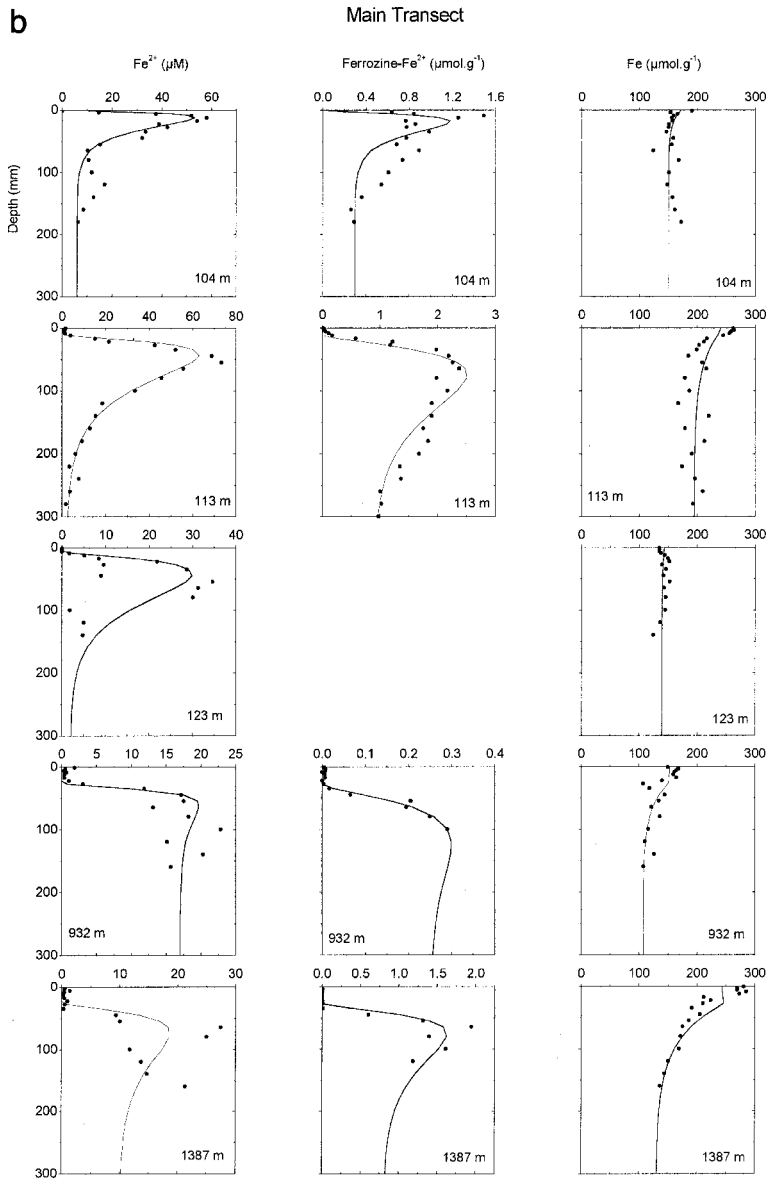

Figure 8. (Continued)

similar to those estimated for the North Sea with a simpler model and without data on ferrozine-extractable Fe^{2+} (Slomp *et al.*, 1997). The values for the first order rate constants are comparable to those obtained for Mn cycling at the Iberian margin, whereas the estimated Fe(III) deposition fluxes are higher than those for Mn(IV) (Van der Zee *et al.*,

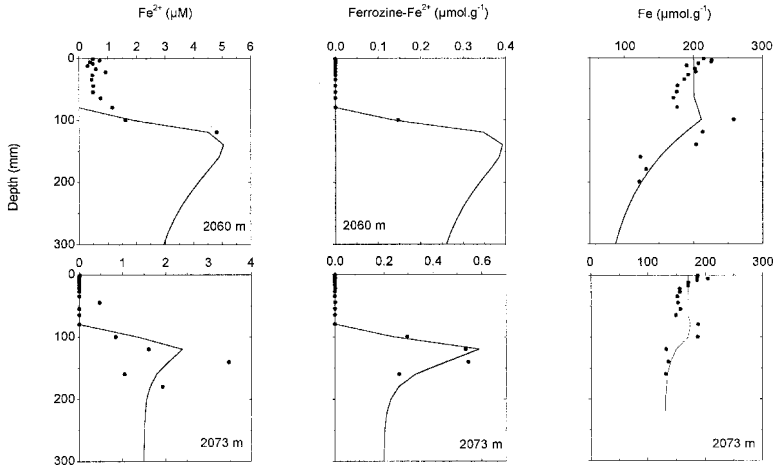

Figure 8. (Continued)

2001). Integrated rates of reaction were calculated directly from the model results (Table 5). At the non-canyon stations, depth-integrated reduction and oxidation rates are highest and most variable for stations shallower than 400 m, decrease with increasing water depth and are close to zero deeper than ~2200 m (Fig. 9). At the 344-m station in the head of the canyon, depth-integrated rates of Fe(III) reduction and Fe(II) oxidation are similar to other shallow water stations, but higher than at the 396-m station on the adjacent shelf. In the canyon, integrated rates of Fe(III) reduction and Fe(II) oxidation increase with water depth until a maximum is reached at the 3097-m station at the basis of the canyon. At the 4280-m station in the fan of the canyon the rates are lower again, yet relatively high as compared with stations on the abyssal outside the canyon.

7. Discussion

a. Role of loosely sorbed Fe^{2+} in Fe cycling

Ferrozine-extractable Fe^{2+} is assumed to represent Fe(II) loosely sorbed to the sediment. We tried to model this pool with the approach of instaneous equilibrium sorption (Berner, 1976; Schink and Guinasso, 1978) of dissolved Fe^{2+} and the linear sorption coefficient $Ks = 1$ (Slomp *et al.,* 1997). The thus calculated amount of sorbed $Fe^{2+} = K_s \times [Fe^{2+}]$ could account only for a few percent of the measured ferrozine-extractable Fe^{2+} in the sediment. Also, it could not reproduce the shape of the depth distributions. Where the pore water Fe^{2+} concentration decreases due to precipitation with sulfides, ferrozine-extractable Fe^{2+} does not decline concurrently, suggesting that dissolved Fe^{2+} precipitates without replenishment through Fe^{2+} desorption from the solid phase. The consumption of loosely sorbed Fe^{2+} can be accomplished via 2 pathways; (1) Fe^{2+} is released into the pore water, where it is rapidly precipitated so that dissolved Fe^{2+} cannot

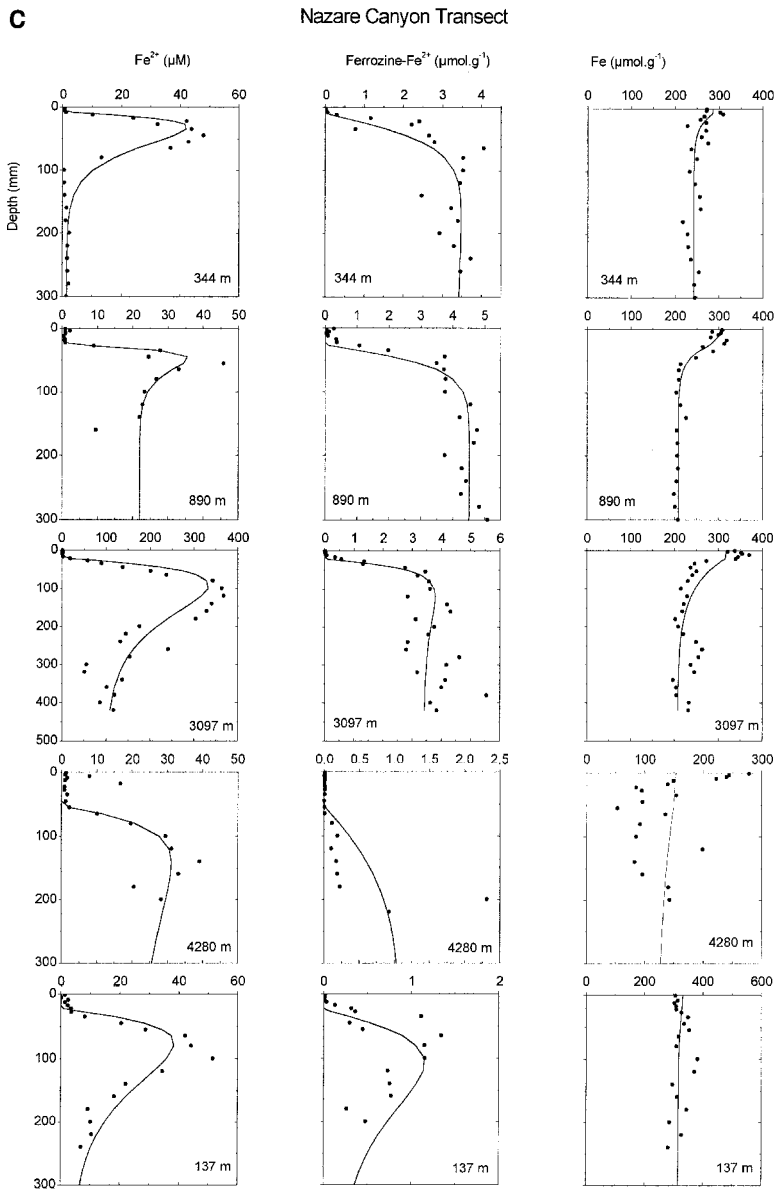

Figure 8. (Continued)

accumulate, and (2) loosely sorbed Fe^{2+} may transform directly into a new ferrous phase with the sediment matrix acting as a template. In the first pathway, slow desorption of Fe^{2+} is the rate limiting step in the precipitation of dissolved Fe^{2+} into ferrous minerals. The shift from the adsorption dominated Fe^{2+} production zone to the desorption dominated

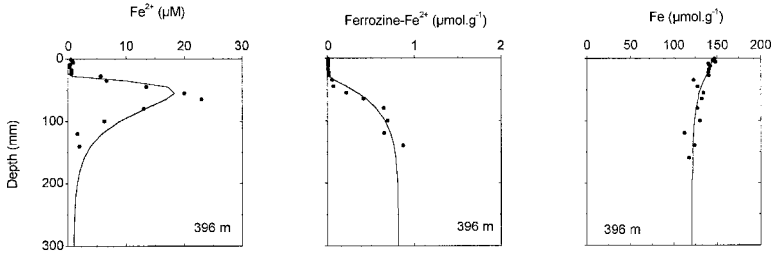

Figure 8. (Continued)

precipitation zone would then explain the more rapid decrease of dissolved Fe^{2+} with depth in the pore water than that of ferrozine-extractable Fe^{2+}. In the second pathway, there are two distinct precipitation mechanisms, one where reduced compounds precipitate from solution and a second involving a heterogeneous reaction each with their own kinetics. In our test of the extraction procedure, ferrozine recovered only about one-third of the added Fe^{2+} implying that the major portion of the added Fe^{2+} was bound firmly to surfaces of the reduced sediment matrix within 30 minutes, thereby becoming unavailable for the ferrozine extraction. This suggests that adsorption, possibly followed by precipitation, rather than desorption controls the ferrozine-extractable pool of Fe^{2+}.

Table 4. Values for k_r, k_s, k_a, k_p and $J_{Sx=0}$ obtained by fitting the model to the data.

Water depth (m)	k_r (d^{-1})	k_{ads} (d^{-1})	k_a (d^{-1})	k_p (d^{-1})	$J_{Sx=0}$ ($\mu mol.m^{-2}.d^{-1}$)
I La Coruña Transect					
175	2.0E-4	3.5E-3	0	2.6E-4	34
2109	1.51E-5	—	5.88E-4	—	10
II Vigo Transect					
223	3.8E-5	1.2E-1	0	1.2E-3	71
III Main Transect					
104	1.4E-3	4.4E-1	0	1.1E-2	481
113	2.1E-4	3.2E-2	4.3E-2	4.2E-4	254
123	5.7E-4	—	2.4E-2	—	56
932	2.9E-5	2.6E-3	2.0E-1	1.5E-5	40
1387	8.7E-6	3.9E-2	1.9E-11	3.6E-4	50
2060	2.3E-6	1.0E-2	5.3E-2	1.8E-4	34
2073	1.3E-5	2.0E-1	0	5.2E-4	29
IV Nazaré Canyon Transect					
137	7.7E-5	5.7E-3	0	8.0E-5	57
396	1.3E-4	4.6E-3	8.4E-2	5.3E-7	97
344	4.0E-4	4.2E-3	3.5E-2	1.0E-5	446
890	2.8E-4	1.7E-2	2.0E-1	1.0E-9	122
3097	8.0E-5	1.4E-3	6.3E-3	8.1E-4	566
4280	3.5E-6	9.8E-4	1.3E-2	8.1E-7	63

Table 5. Calculated integrated rates of reduction, sorption, oxidation, precipitation and burial of Fe from the model results.

Water depth (m)	Reduction (μmol. $m^{-2}.d^{-1}$)	Sorption (μmol. $m^{-2}.d^{-1}$)	Oxidation (μmol.$m^{-2}.d^{-1}$)		Precipitation (μmol.$m^{-2}.d^{-1}$)		Burial Fe (μmol. $m^{-2}.d^{-1}$)
			$Fe^{2+}_{(aq)}$	$Fe^{2+}_{(ads)}$	$Fe^{2+}_{(aq)}$	$Fe^{2+}_{(ads)}$	
La Coruña Transect							
175	17	4	12	4	0	0	34
2109	8	—	7.4	—	0.3	—	10
4908	#	#	#	#	#	#	#
4941	#	#	#	#	#	#	#
Vigo Transect							
213	—	—	—	—	—	—	—
223	63	56	8	7	0	49	23
2164	#	#	#	#	#	#	#
2213	#	#	#	#	#	#	#
2926	#	#	#	#	#	#	#
2932	#	#	#	#	#	#	#
3371	#	#	#	#	#	#	#
Main Transect							
104	599	454	53	87	0	368	21
113	364	117	89	45	158	72	23
123	65	—	34	—	31	—	24
932	41	0.2	27	0.1	14	0	26
1387	41	24	18	1	0	23	27
2060	29	4	5	0	20	4	10
2073	11	7	5	0	0	7	22
2853	#	#	#	#	#	#	#
Nazaré Canyon Transect							
137	42	17	25	4	0	13	44
396	87	3	23	3	61	0	36
344	177	9	96	4	72	0	369
890	198	7	99	7	91	0	30
3097	426	41	191	30	194	5	361
4280	25	1	7	0	17	1	45

Most likely zero, not able to determine

Close to the redox boundary, upon Fe reduction, Fe^{2+} is released into the pore water and subsequently bound to the sediment. Pore water Fe^{2+} can diffuse and solid Fe(II) including ferrozine-extractable Fe^{2+} can be mixed up into the oxic layer where they will be re-oxidized or transported deeper into the sediment, where they will transform into authigenic ferrous minerals. Dissolved Fe^{2+} is transported faster due to molecular diffusion than solid Fe(II), which is transported by diffusive mixing. Pore water Fe^{2+} concentrations can decline very rapidly, leading to a sharply defined zone of authigenic

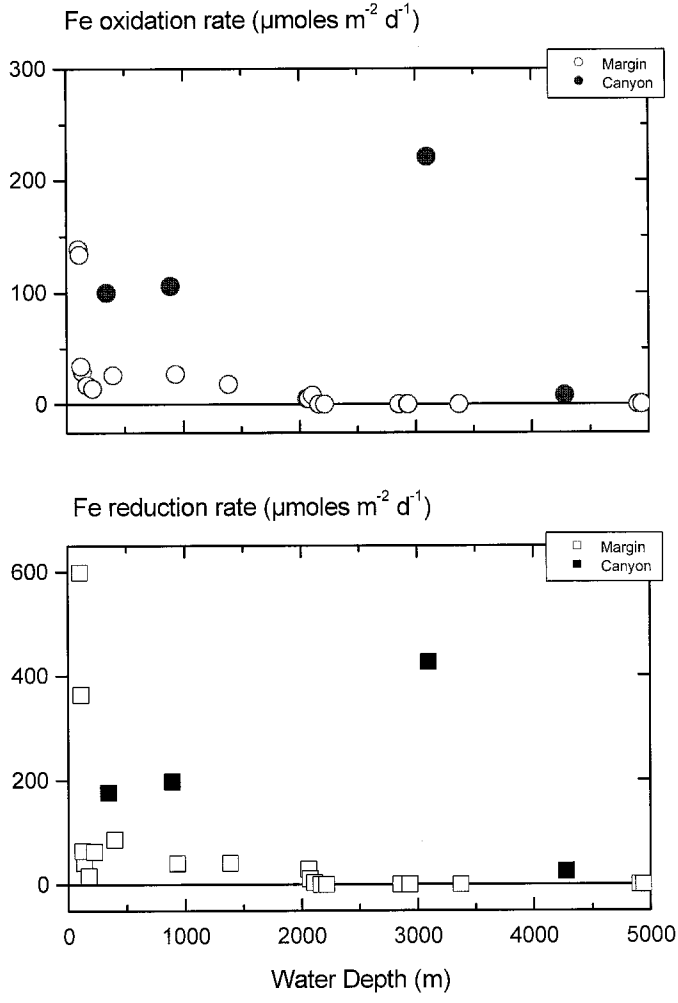

Figure 9. Fe^{2+} oxidation rate (circles) and Fe reduction rate (squares) as a function of water depth on the margin (open symbols) and in the canyon (filled symbols).

ferrous mineral formation. Through association with the sediment matrix, the authigenic ferrous mineral formation is partly delayed. The ferrozine-extractable Fe^{2+} is transported deeper into the sediment than dissolved Fe^{2+} is, so that it can act as a deep source for authigenic ferrous mineral formation. Thamdrup *et al.* (1994) measured profiles of non-S-bound Fe(II) that was involved in FeS formation, because its concentration decreased with increasing FeS content. Their non-S-bound Fe(II) is distributed like their pore water Fe^{2+} and our ferrozine-extractable Fe^{2+} profiles. On the Chilean slope, non-S-bound Fe(II) was the largest Fe(II) pool measured in the solid phase, exceeding pyrite 5-fold (Thamdrup and Canfield, 1996). Canfield *et al.* (1993) also report a large

non-S-bound Fe(II) pool in North Sea sediments, representing more than 50% of the Fe(II) in the solid phase and suggest it could be bound in Fe carbonates or adsorbed onto sediment particles. Wang and Van Cappellen (1996) used these data in their STEADYSED model and attributed non-S-bound Fe(II) largely to adsorbed Fe^{2+} and a minor fraction to siderite ($FeCO_3$). Their estimates showed that the main oxidation pathway is heterogeneous, i.e. via oxygenation of adsorbed Fe^{2+}. Although, it is very likely that ferrozine-extractable Fe^{2+} will be rapidly oxidized, it is not possible to extract information about the preferred oxidation pathway from our data.

b. Substrates for Fe^{2+} sorption

Both microbial and abiotic reduction of Fe oxides are surface-controlled processes (Nevin and Lovley, 2000; Stumm and Sulzberger, 1992) and Fe^{2+} sorption may therefore affect the reduction rate. Adsorbed or precipitated Fe^{2+} on the surface of goethite was found to limit the rate and extent of dissimilatory Fe(III) reduction by bacteria (Roden *et al.,* 1996, 1999), but goethite was reduced more readily in the presence of aluminum oxide, due to sorption of Fe^{2+} to the Al oxide surface (Urrutia *et al.,* 1999). Hence, aluminium oxides and layered silicates have been suggested as alternate sinks for Fe^{2+} in the sediment. Sorption of Fe^{2+} complexed by organic ligands may facilitate electron transfer at the Fe oxide surface, thus enhancing the Fe(III) reduction rate, as the Fe^{2+} in the bridging ligands catalyze the reductive dissolution reaction (Luther III *et al.,* 1992; Stumm, 1992). We did not observe a positive or negative correlation between the ferrozine-extractable Fe^{2+} content and Fe(III) reduction rates at the Iberian margin. However, stations with ferrozine-extractable Fe^{2+} contents higher than 1 μmol g^{-1} also have a relatively high C_{org} content (Table 1). Thus, Fe^{2+} might sorb onto Fe(III) minerals after complexation by organic compounds or particulate organic matter, without inhibiting Fe reduction.

c. The rate controlling factor for Fe cycling

The organic carbon mineralization rates are highest at the shelf (see Research Area). Fe reaction rates are highest at the shelf as well, decreasing with increasing water depth at the non-canyon stations. Turnover times were estimated from the standing stock divided by the production rate for the pore water Fe^{2+}, ferrozine-extractable Fe^{2+} and solid phase Fe in both the oxidized and the reduced layer. The highest turnover time was found for solid phase Fe in the oxidized layer for all stations, except for the 2060-m station on the main transect, where the solid phase Fe in the reduced layer has a slightly longer turnover time. Pore water and ferrozine-extractable Fe^{2+} had 2–6 orders of magnitude shorter turnover times. We conclude that the rate-limiting step in the sedimentary Fe redox cycle is the transfer of solid phase Fe from the oxidized to the reduced layer. Thus, solid phase mixing limits Fe cycling at the Iberian margin. Sediment mixing is necessary to bring Fe oxyhydroxides into the reduced layer and to stimulate anoxic organic carbon mineralization by burial of reactive organic matter (Aller, 1986). Dhakar and Burdige (1996) simulated the effect of increasing bioturbation on their model determined depth-integrated rates of oxic and sub-oxic (nitrate, manganese(IV) and iron(III) as electron acceptors)

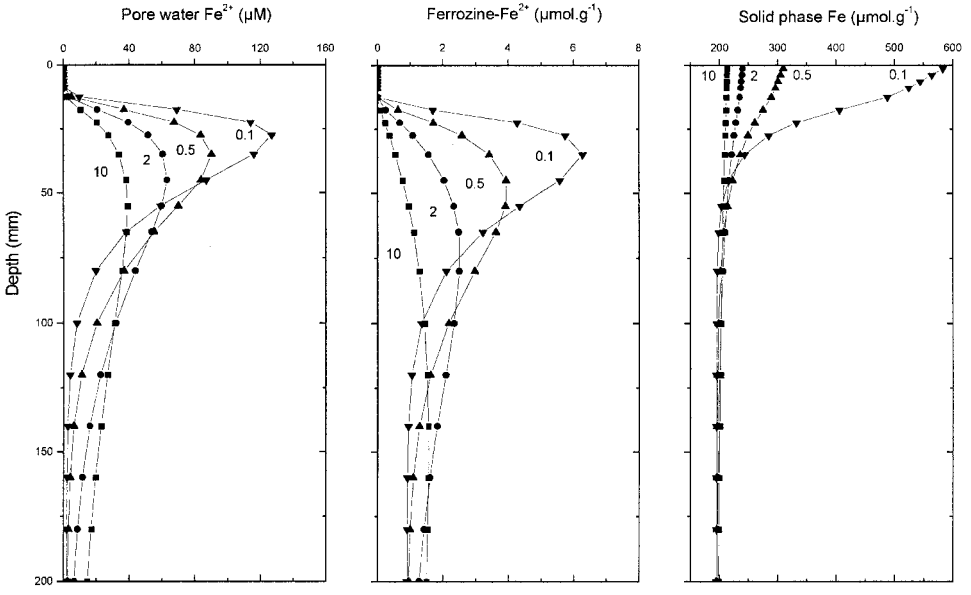

Figure 10. Effect of varying the mixing coefficient (values are in $cm^2\ yr^{-1}$) on the pore water Fe^{2+}, ferrozine-extactable Fe^{2+} and solid phase Fe profiles of the 113-m station at the main transect.

organic carbon mineralization rates and showed that with increasing mixing rate sub-oxic respiration increased while the total areal carbon mineralization remained constant.

The effect of changing the mixing coefficient (D_b) on the Fe profiles of the 113-m station on the main transect, while keeping the other parameters in Table 3 and 4 constant, is shown in Figure 10. Pore water Fe^{2+}, ferrozine-extractable Fe^{2+} and solid phase Fe profiles show increasing maxima with decreasing values of D_b. Thus as expected, mixing smoothes the profiles. To assess the influence of sediment mixing on the homogeneous and heterogeneous oxidation and reduction rates, the Fe profiles of the 113-m station on the main transect were fitted with varying D_b values (Fig. 11), while keeping the other input parameters constant (Table 3). Enhanced mixing increased both the oxidation and the reduction rate, confirming the importance of sediment mixing in Fe cycling. Moreover, the results showed that heterogeneous oxidation becomes more important with enhanced sediment mixing. This analysis probably underestimates the heterogeneous contribution to the oxidation of Fe(II), because the same oxidation rate constant (k_{ox} is 10 d^{-1}) is used for both the pore water and the ferrozine-extractable Fe^{2+}, whereas heterogeneous oxidation is likely to be the more rapid pathway (Stumm and Sulzberger, 1992).

d. Canyon vs. Margin—The influence of the bulk sediment accumulation rate

The three transects over the margin show the same decreasing trend in Fe oxidation and reduction rates with water depth, whereas the rates in the Nazaré canyon transect slightly

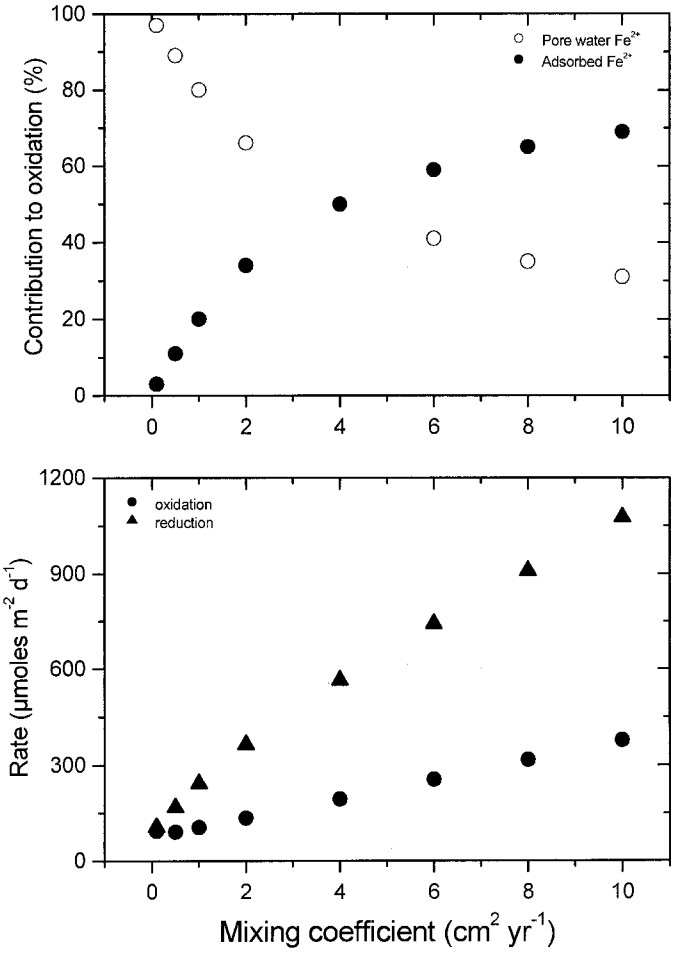

Figure 11. Effect of varying the mixing coefficient on pore water Fe^{2+} and ferrozine-extractable Fe^{2+} oxidation rates and Fe reduction rates of the 113-m station at the main transect.

increase with depth until the basis at 3097 m. The organic carbon mineralization rates decrease with water depth both in the canyon as well as outside the canyon (Epping *et al.*, 2002). At the 344-m station in the head of the canyon, the organic carbon mineralization rate and the Fe reduction rate are well within the range found for the shelf stations. However, while the organic carbon mineralization rate is a factor three higher at the 3097-m canyon basis, the Fe reduction rate is several orders of magnitude higher than at similar water depth outside the canyon. The deposition fluxes obtained from the model fits (Table 4) show enhanced Fe deposition at the 344-, 890- and 3097-m stations in the canyon compared to stations on the margin at similar water depths. The Nazaré canyon focuses sediment and transports it from the shelf directly to the deep sea (Smith *et al.*, 2001). The

bulk sediment accumulation rate in the canyon is largest at its basis at 3097 m, and one order of magnitude higher than on the shelf (Van Weering *et al.,* 2002). The organic carbon mineralization rate, however, is lower at 3097 m in the canyon than at the shallow stations on the shelf. Thus rather than high mineralization activity, the high bulk sediment accumulation rate associated with sediment focusing by the canyon is likely the driving force for the maximum Fe reduction at the 3097-m canyon station.

e. Iberian margin vs. the world

Thamdrup and Canfield (1996) argued that a substantial contribution of Fe reduction in the organic matter oxidation could be widespread on continental margins, because O_2 and NO_3^- penetration into shelf and slope sediments is only a few mm's to cm's (Reimers *et al.,* 1992; Brandes and Devol, 1995). Using bag incubations the contribution of Fe reduction to the mineralization has been estimated up to 29% on the Chilean continental margin (Thamdrup and Canfield, 1996), 25% in a high-latitude Arctic fjord in Greenland (Rysgaard *et al.,* 1998) and up to 51% in the Skagerrak (Canfield *et al.,* 1993). However, bag incubations tend to stimulate and therefore overestimate anoxic processes, due to the depletion of O_2 and NO_3^- during incubation (Thamdrup and Canfield, 1996). Estimates from pore water profile modeling indicated that Fe reduction is less important (<2%) at the Canadian and central Californian continental margins (Boudreau *et al.,* 1998; Reimers *et al.,* 1992), and <4% at the North Sea continental margin, with the exception of the Skagerrak ~ 20% (Slomp *et al.,* 1997). Pore water profile-derived estimates are likely too low, because an unknown amount of Fe^{2+} is adsorbed to the solid phase (Canfield *et al.,* 1993). Therefore, we choose to estimate Fe reduction rates from simultaneous modeling of pore water Fe^{2+}, loosely sorbed Fe^{2+} and solid phase Fe profiles. Assuming 1C : 4Fe stoichiometry for C_{org} oxidation : Fe reduction, the contribution of the reduction of Fe to organic carbon mineralization is 5% at the 104-m and 113-m stations on the main transect and 6% the 3097-m station in the canyon, and less than 4% at the remaining stations. The data for the 3097-m station in the canyon indicated that apart from mineralization activity, deposition of sufficient reactive Fe is a crucial factor determining Fe reduction rates. We conclude that the sediments of the Iberian margin contain insufficient reactive Fe(III) to allow for an important role of Fe reduction in organic carbon mineralization. Other solid phase ferrous compounds, which have higher concentrations than ferrozine-extractable Fe^{2+}, are important for Fe cycling as well (e.g. Canfield *et al.,* 1993; Thamdrup *et al.,* 1994; Thamdrup and Canfield, 1996). Estimates of Fe reduction rates can be further improved by including all ferrous phases in diagenetic models. Upon mixing into the oxic layer, they are re-oxidized supplying Fe(III) and their recycling rate will be enhanced with sediment mixing similar to ferrozine-extractable Fe^{2+}.

8. Conclusions

Close to the redox boundary, Fe^{2+} is released into the pore water upon Fe reduction, and subsequently either sorbed onto the sediment matrix and/or precipitated to form authigenic

ferrous minerals. Deeper down in the sediment, the loosely sorbed Fe^{2+} may be released again, however, without the accumulation of dissolved Fe^{2+} due to its immediately precipitation or be directly transformed into other authigenic Fe(II) phases. Thus, adsorbed Fe^{2+} acts as a deep source for authigenic ferrous mineral formation. Fe oxidation and reduction rates decreased with water depth at the non-canyon stations of the Iberian margin. At the shelf, organic carbon mineralization rates are highest and drive the Fe cycle. In the canyon, the high deposition fluxes drive the Fe cycle. The highest contributions of Fe(III) reduction to the overall organic matter oxidation are 5% at the 104-m and 113-m stations on the main transect and 6% at the 3097-m deposition station in the canyon. The rate-limiting factor for Fe cycling, as deduced from the turnover times, is sediment mixing. Model simulations showed that heterogeneous oxidation becomes relatively more important with increased sediment mixing.

Acknowledgments. For Wim. We miss you. On November 6, 2002, Wim van Raaphorst died in a traffic accident while biking home from NIOZ.

The authors wish to thank the captain and crew of R. V. *Pelagia* for providing safe cruises and a pleasant working environment. Shipboard nitrate and iron analyses were performed by Karel Bakker, Jan van Ooijen and Evaline van Weerlee (NIOZ, department of Marine Chemistry and Geology). We thank Eric Epping for very kindly providing the nitrate data. Two anonymous referees and the Associate Editor, Don Rice, are thanked for their comments, which greatly helped us to improve the manuscript. The investigations were carried out in the framework of the Sedimentary Manganese and Iron cycLEs (SMILE) program that was supported by the Research Council for Earth and Life Science (ALW) with financial aid from the Netherlands Organization for Scientific Research (NWO) (no. 750.297.01). W.H. was supported through a grant by the European community EC-MAST OMEX-II project (MAS3-CT96-0056). This is publication no. 3517 of the Netherlands Institute for Sea Research.

APPENDIX

Solutions to differential equations

$$C_I = B_1 \exp(e_1 x) + B_2 \exp(e_2 x) \tag{A1}$$

$$A_I = F_1 \exp(e_3 x) + F_2 \exp(e_4 x) \tag{A2}$$

$$S_I = G_1 + G_2 \exp\left(\frac{\omega x}{D_b}\right) + \alpha B_1 \exp(e_1 x) + \beta B_2 \exp(e_2 x) - F_1 \exp(e_3 x) - F_2 \exp(e_4 x) \tag{A3}$$

$$C_{II} = J \exp(e_{10} x) + \gamma H \exp(e_6 x) + C_a \tag{A4}$$

$$A_{II} = I \exp(e_8 x) + \delta J \exp(e_{10} x) + \varepsilon H \exp(e_6 x) + A_{eq} \tag{A5}$$

$$S_{II} = H \exp(e_6 x) + S_{eq} \tag{A6}$$

$$e_1 = \frac{\omega + \sqrt{\omega^2 + 4[D_b + D_s]k_{oxc}}}{2[D_b + D_s]} \tag{A7}$$

$$e_2 = \frac{\omega - \sqrt{(\omega^2 + 4[D_b + D_s]k_{oxc}}}{2[D_b + D_s]} \tag{A8}$$

$$e_3 = \frac{\omega + \sqrt{\omega^2 + 4D_b k_{oxa}}}{2D_b} \quad e_4 = \frac{\omega - \sqrt{\omega^2 + 4D_b k_{oxa}}}{2D_b} \tag{A9 \& A10}$$

$$e_6 = \frac{\omega - \sqrt{\omega^2 + 4D_b k_r}}{2D_b} \quad e_8 = \frac{\omega - \sqrt{\omega^2 + 4D_b k_p}}{2D_b} \tag{A11 \& A12}$$

$$e_{10} = \frac{\omega - \sqrt{\omega^2 + 4D_b k_a}}{2D_b} \tag{A13}$$

$$\alpha = \frac{-k_{oxc}}{\theta[D_b e_1^2 - \omega e_1]} \quad \beta = \frac{-k_{oxc}}{\theta[D_b e_2^2 - \omega e_2]} \tag{A14}$$

$$\gamma = \frac{k_r \theta}{[D_b + D_s]e_6^2 - \omega e_6 - (k_a + k_{ads})} \tag{A15}$$

$$\delta = \frac{-k_{ads}}{\theta(D_b e_{10}^2 - \omega e_{10} - k_p)} \quad \varepsilon = \frac{-k_{ads}\gamma}{\theta(k_r - k_p)} \tag{A16 \& A17}$$

The integration constants (B_1, B_2, F_1, F_2, G_1, G_2, J, H and I) were analytically solved with the following boundary conditions:

When $x = 0$

$$C_I = C_0$$

$$J_{Ax=0} = 0$$

$$J_{Sx=0} = -\phi\theta(D_b A_1' - \omega A_1)$$

When $x = L$

$$C_I = C_{II}$$

$$A_I = A_{II}$$

$$S_I = S_{II}$$

$$[D_b + D_s]C_1' - \omega C_I = [D_b + D_s]C_{II}' - \omega C_{II}$$

$$D_b A_1' - \omega A_I = D_b A_{II}' - \omega A_{II}$$

$$D_b S_I' - \omega S_I = D_b S_{II}' - \omega S_{II}$$

When $x \to \infty$

$$C_{II} = C_a,$$

$$A_{II} = A_{eq}$$

$$S_{II} = S_{eq}$$

REFERENCES

Aller, R. C. 1980. Diagenetic processes near the sediment-water interface of Long Island Sound II. Fe and Mn. Adv. Geophys., *22,* 351–415.

Aller, R. C., J. E. Mackin and R. T. Cox, Jr. 1986. Diagenesis of Fe and S in Amazon inner shelf muds: apparent dominance of Fe reduction and implications for the genesis of ironstones. Cont. Shelf Res., *6,* 263–289.

Berner, R. A. 1976. Inclusion of adsorption in the modelling of early diagenesis. Earth Plan. Sci. Lett., *29,* 333–340.

Boudreau, B. P., A. Mucci, B. Sundby, G. W. Luther and N. Silverberg. 1998. Comparative diagenesis at three sites on the Canadian continental margin. J. Mar. Res., *56,* 1259–1284.

Brandes, J. A. and A. H. Devol. 1995. Simultaneous nitrate and oxygen respiration in coastal sediments: Evidence for discrete diagenesis. J. Mar. Res., *53,* 771–797.

Burdige, D. J. and J. M. Gieskes. 1983. A pore water/solid phase diagenetic model for manganese in marine sediments. Am. J. Sci., *283,* 29–47.

Burdige, D. J. and P. E. Kepkay. 1983. Determination of bacterial manganese oxidation rates in sediments using a in-situ dialysis technique, I. Laboratory studies. Geochim. Cosmochim. Acta, *47,* 1907–1916.

Canfield, D. E. 1988. Dissertation. Sulfate reduction and the diagenesis of iron in anoxic marine sediments. Yale University, New Haven CT.

Canfield, D. E., B. Thamdrup and J. W. Hansen. 1993. The anaerobic degradation of organic matter in Danish coastal sediments: Iron reduction, manganese reduction and sulfate reduction. Geochim. Cosmochim. Acta, *57,* 3867–3883.

Dhakar, S. P. and D. J. Burdige. 1996. A coupled non-linear, steady state model for early diagenetic processes in pelagic sediments. Am. J. Sci., *296,* 296–330.

Dollhopf, M. E., K. H. Nealson, D. M. Simon and G. W. Luther III. 2000. Kinetics of Fe(III) and Mn(IV) reduction by the black sea strain of *Shewanella putrefaciens* using in situ solid state voltametric Au/Hg electrodes. Mar. Chem., *70,* 171–180.

Durieu de Madron, X., P. Castaing, F. Nyffeler and T. Courp. 1999. Slope transport of suspended particulate matter on the Aquitanain margin of the Bay of Biscay. Deep-Sea Res. II, *46,* 2003–2027.

Epping, E., C. Van der Zee, K. Soetaert and W. Helder. 2002. On the mineralisation and burial of organic carbon in sediments of the Iberian margin and Nazaré Canyon (NE Atlantic). Progr. Oceanogr., *52,* 399–431.

Hansen, H. C. B., O. K. Borggaard and J. Sørensen. 1994. Evaluation of the free energy of formation of Fe(II)-Fe(III) hydroxide-sulphate (green rust) and its reduction of nitrite. Geochim. Cosmochim. Acta, *58,* 2599–2608.

Koch, C. B. and S. Mørup. 1991. Identification of GR in an ochre sludge. Clay Mineral., *26,* 577–582.

Kostka, J. E. and G. W. Luther III. 1994. Partitioning and speciation of solid phase iron in saltmarsh sediments. Geochim. Cosmochim. Acta, *58,* 1701–1710.

Lovley, D. R. and E. J. P. Phillips. 1986. Organic matter mineralization with reduction of ferric iron in anaerobic sediments. Appl. Environ. Microbiol., *51,* 683–689.

——— 1988. Novel mode of microbial energy metabolism: Organic carbon oxidation coupled to the dissimilatory reduction of iron and manganese. Appl. Environ. Microbiol., *54,* 1472–1480.

Luther III, G. W., J. E. Kostka, T. M. Church, B. Sulzberger and W. Stumm. 1992. Seasonal iron cycling in the salt-marsh sedimentary environment: the importance of ligand complexes with Fe(II) and Fe(III) in the dissolution of Fe(III) minerals and pyrite, respectively. Mar. Chem., *40,* 81–103.

Luther III, G. W., P. A. Shellenbarger, and P. J. Brendel. 1996. Dissolved organic Fe(III) and Fe(II) complexes in salt marsh porewaters. Geochim. Cosmochim. Acta, *60*, 951–960.

Monaco, A., X. Durrieu de Mardon, O. Radakovitch, S. Heussner and J. Carbonne. 1999. Origin and variability of downward biogeochemical fluxes on the Rhone continental margin (NW Mediterranean). Deep-Sea Res. I., *46*, 1483–1511.

Nevin, K. P. and D. R. Lovley. 2000. Lack of production of electron-shuttling compounds or solubilization of Fe(III) during reduction of insoluble Fe(III) oxide by *Geobacter metallireducens*. Appl. Environ. Microbiol., *66*, 2248–2251.

Reimers, C. E., R. A. Jahnke and D. C. McCorkle. 1992. Carbon fluxes and burial rates over the continental slope and rise off central California with implications for the global carbon cycle. Global Biogeochem. Cycles, *6*, 199–224.

Rickard, D. 1995. Kinetics of FeS precipitation: Part 1. Competing reaction mechanisms. Geochim. Cosmochim. Acta, *59*, 4367–4379.

Roden, E. E. and M. M. Urrutia. 1999. Ferrous iron removal promotes microbial reduction of crystalline iron (III) oxides. Environ. Sci. Technol., *33*, 1847–1853.

Roden, E. E. and J. M. Zachara. 1996. Microbial reduction of crystalline iron(III) oxides: Influence of oxide surface area and potential for cell growth. Environ. Sci. Technol., *30*, 1618–1628.

Rysgaard, S., B. Thamdrup, N. Risgaard-Petersen, H. Fossing, P. Berg, P. B. Christensen and T. Dalsgaard. 1998. Seasonal carbon and nutrient mineralisation in a high-Arctic coastal marine sediment, Young Sound, Northeast Greenland. Mar. Ecol. Progr. Ser., *175*, 261–276.

Sanchez-Cabeza, J. A., P. Masqué, I. Ani-Ragolta, J. Merino, M. Frignani, F. Alvisi, A. Palanques and P. Puig. 1999. Sediment accumulation rates in the southern Barcelona continental margin (NW Mediterranean Sea) derived from 210Pb and 137Cs chronology. Progr. Oceanogr., *44*, 213–332.

Schink, D. R. and N. L. Guinasso. 1978. Redistribution of dissolved and adsorbed materials in abyssal marine sediments undergoing biological stirring. Am. J. Sci., *278*, 687–702.

Schmidt, S., T. C. E. Van Weering, H. C. De Stigter. 2001. Enhanced short-term deposition within the Nazaré Canyon, North-East Atlantic. Mar. Geol., *173*, 55–67.

Slomp, C. P., J. F. P. Malschaert, L. Lohse and W. Van Raaphorst. 1997. Iron and manganese cycling in different sedimentary environments on the North Sea continental margin. Cont. Shelf Res., *17*, 1083–1117.

Stampfl, P. P. 1969. Ein basisches Eisen-II-III-karbonate. Rost. Corros. Sci., *9*, 185–187.

Sørensen, J. 1982. Reduction of ferric iron in anaerobic, marine sediment and interaction with reduction of nitrate and sulfate. Appl. Environ. Microbiol., *43*, 319–324.

Stookey, L. L. 1970. A new spectrophotometric reagent for iron. Anal. Chem., *42*, 779–781.

Stumm, W. 1992. Chemistry of the solid-water interface: Processes at the mineral-water and particle-water interface in natural systems. Wiley NY, 428 pp.

Stumm, W. and B. Sulzberger. 1992. The cycling of iron in natural environments: Considerations based on laboratory studies of heterogeneous redox processes. Geochim. Cosmochim. Acta, *56*, 3233–3257.

Thamdrup, B. and D. E. Canfield. 1996. Pathways of carbon oxidation in continental margin sediments off central Chile. Limnol. Oceanogr., *41*, 1629–1650.

Thamdrup, B., H. Fossing and B. B. Jørgensen. 1994. Manganese, iron, and sulfur cycling in a coastal marine sediment, Aarhus Bay, Denmark. Geochim. Cosmochim. Acta, *58*, 5115–5129.

Tessier, A., P. G. C. Campbell and M. Bisson. 1979. Sequential extraction procedure for the speciation of particulate trace metals. Anal. Chem., *51*, 844–851.

Tessier, A., D. Fortin, N. Belzile, R. R. DeVitre and G. G. Leppard. 1996. Metal sorption to diagenetic iron and manganese oxyhydroxides and associated organic matter: Narrowing the gap between field and laboratory measurements. Geochim. Cosmochim. Acta, *60*, 387–404.

Trolard, F., J.-M. R. Génin, M. Abdelmoula, G. Boerrié, b. Humbert and A. Herbillon. 1997.

Identification of a green rust mineral in a reductomorphic soil by Mössbauer and Raman spectroscopies.Geochim. Cosmochim. Acta, *61,* 1107–1111.

Tügel, J. B., M. E. Hines and G. E. Jones. 1986. Microbial iron reduction by enrichment cultures isolated from estuarine sediments. Appl. Environ. Microbiol., *52,* 1167–1172.

Urrutia, M. M., E. E. Roden and J. M. Zachara. 1999. Influence of aqueous and solid-phase Fe(II) complexants on microbial reduction of crystalline iron (III) oxides. Environ. Sci. Technol., *33,* 4022–4028.

Van Cappellen, P. and Y. Wang. 1995. Metal cycling in surface sediments: Modeling the interplay between transport and reaction, *in* Metal contaminated aquatic sediments, H. E. Allen, eds., Ann Arbor Press, 21–64.

—— 1996. Cycling of iron and manganese in surface sediments: a general theory for the coupled transport and reaction of carbon, oxygen, nitrogen, sulfur, iron, and manganese. Am. J. Sci., *296,* 197–243.

Van der Zee, C., W. van Raaphorst, E. Epping. 2001. Adsorbed Mn^{2+} and Mn redox cycling in Iberian continental margin sediments (North East Atlantic). J. Mar. Res., *59,* 133–166.

Van Weering, T. C. E., H. C. De Stigter, W. Boer and H. De Haas. 2002. Recent sediment transport and accumulation at the western Iberian margin. Progr. Oceanogr., *52,* 349–371.

Wallmann, K., K. Hennies, I. Konig, W. Petersen and H-D. Knauth. 1993. New procedure for determining reactive Fe(III) and Fe(II) minerals in sediments. Limnol. Oceanogr., *38,* 1803–1812.

Wang, Y. and P. Van Cappellen. 1996. A multicomponent reactive transport model of early diagenesis: Application to redox cycling in coastal marine sediments. Geochim. Cosmochim. Acta, *60,* 2993–3014.

Zhang, H., W. Davison, S. Miller and W. Tych. 1995. In situ high resolution measurements of fluxes of Ni, Cu, Fe and Mn and concentrations of Zn and Cd in porewaters by DGT. Geochim. Cosmochim. Acta, *59,* 4181–4192.

Received: *11 September, 2000;* revised *19 November, 2002.*